

The 3-Mode Coherence Sector

Ontic Foundations of Generational Structure, Mixing, and CP
Violation in the Coherence-Relational Blockworld

Chet Braun

Braun Science & Engineering

April 2026

DOI: 10.5281/zenodo.19872905

V1.0

Abstract

The Standard Model flavor sector—three generations of quarks and leptons, hierarchical masses, nontrivial mixing matrices, and CP-violating phases—remains empirically successful but lacks a unifying structural account. In the Coherence-Relational Blockworld (cRBW) [1] and its Mathematical Model (MM) [2], physical structure is determined by global relational constraints rather than dynamical evolution. Within this framework, we examine the minimal internal structure required to support nontrivial holonomy, CP-odd invariants, and closure-consistent relational asymmetry under the Boundary-of-Boundaries principle (BBP), No Preferred Reference Frame (NPRF), and the Relational Coherence Conditions (RCC).

We show that a three-mode internal coherence sector is the minimal dimensionality supporting nontrivial $SU(3)_{\text{coh}}$ -type holonomy and CP-odd invariants, providing a natural structural candidate for organizing flavor phenomena. We then construct an extended capacity-tensor formulation incorporating this sector and define a mixing-selection functional on a capacity-weighted Grassmannian, whose minima are consistent with observed quark and lepton mixing structures.

Within this framework: (i) three-mode coherence is identified as the minimal structure supporting CP-violating invariants and non-Abelian relational closure; (ii) flavor degrees of freedom can be interpreted as representational projections of this internal sector; (iii) an extended geometric-coherence capacity tensor provides a unified setting for mixing, mass hierarchies, and environment-dependent effects; and (iv) a variational mixing-selection principle admits minima consistent with CKM and PMNS mixing patterns, including small quark mixing, large lepton mixing, and nonzero CP violation.

These results do not derive the numerical values of Standard Model parameters, but provide a structural framework in which their qualitative features arise from minimal coherence requirements of a closure-first relational ontology.

Table of Contents

1. Introduction.....	4
2. Minimal Coherence Dimensionality and CP-Odd Structure.....	6
2.1 Minimality of CP-Odd Invariants.....	6
2.2 RCC-2: Relation to Closure and Relational Structure.....	8
2.3 Minimal Non-Abelian Coherence Structure	8
2.4 Grassmannian Perspective	8
2.5 Minimality Statement	9
3. Embedding the 3-Mode Coherence Sector in the Capacity Fiber	10
3.1 Extended Capacity Fiber.....	10
3.2 Admissibility Constraints and Sparsity	11
3.3 Interpretation of Mixed Capacities	11
3.4 Phenomenological Interpretation (Optional Mapping)	11
4. The Coherence Cochain	13
4.1 Definition	13
4.2 Structural Role.....	13
4.3 Coupling to Geometric Structure	13
4.4 Phenomenological Meaning	14
4.5 Relation to Standard Oscillation Structure (Optional Mapping)	14
5. The Mixing-Selection Functional	16
5.1 Mixing as Rotation of Eigenbases	16
5.2 Principal Angles	16
5.3 Capacity-Weighted Metric	16
5.4 Principal-Angle Cost Functional.....	17
5.5 Principal Angle Cost.....	17
5.6 Full Variational Functional	18
5.7 Numerical Consistency Check	19
5.8 Sector Dependence	19
6. Population of Diagonal Capacities (Quarks and ν Sector).....	21
6.1 Quark Sector Diagonals (λ and κ)	21
6.2 Neutrino and charged-lepton eigenvalues	22
6.3 Charged-Lepton Diagonals ($\kappa\ell$)	22
6.4 Combined Observations	23
7. CKM Sector: Mixing Minimization and CP Violation.....	23
7.1 Input: Quark Diagonals.....	23
7.2 Input: CKM Mixing Matrix (PDG 2024)	24
7.3 Variational Behavior	24
7.4 CKM Jarlskog	24

7.5 Interpretation	25
8. PMNS Sector: Mixing Minimization and CP Violation.....	26
8.1 Input: Neutrino Diagonals.....	26
8.2 PMNS mixing angles.....	26
8.3 Minimization Result: PMNS-Like Mixing	26
8.4 PMNS Jarlskog	27
8.5 Interpretation	27
9. Structural Predictions of the 3-Mode Coherence Sector	28
9.1 Consistency with Established Observations	28
9.2 Potential Near-Term Implications	29
9.3 Longer-Term Phenomenological Implications	30
10. Consequences of Reducing Internal Coherence Dimensionality	32
10.1 CP Violation Vanishes	32
10.2 Generational Structure Collapses	32
10.3 Constraints on Closure and Holonomy	32
10.4 Reduced Relational Structure	33
10.5 Interpretation.....	33
11. Conclusion	34
Appendix A — Derivation of the Full 8×8 Capacity Tensor	35
A.1 Review: 5×5 Geometric Capacity Tensor	35
A.2 Expansion to the 3-Mode Coherence Fiber	35
A.3 Why This Tensor is Sparse	36
Appendix B — Mixed-Capacity Support Classes (Extended Table 6').....	37
Appendix C — The Coherence Cochain $\Delta\phi\nu[e]$: Formal Construction in DEC	38
C.1 Definition	38
C.2 Hodge Lifting.....	38
C.3 Phenomenological Role	38
Appendix D — The Jarlskog Scalar in the 3-Mode Sector.....	40
D.1 Decomposition.....	40
D.2 CKM Jarlskog.....	40
D.3 PMNS Jarlskog.....	40
Appendix E — Numeric Values and Tables Used in the Paper.....	42
E.1 Neutrino Masses (NuFit 6.0, NO).....	42
E.2 Neutrino λ Capacities.....	42
E.3 Charged-Lepton κ Capacities	42
E.4 Quark Masses (PDG 2024)	42
E.5 CKM Angles and Jarlskog.....	42
E.6 PMNS Trial Jarlskog	42
E.7 Calculation of J	42
Appendix F — Diagrams	44
F.1 Diagram: 3-Mode Coherence Sector	44
F.2 Diagram: Extended 8×8 Capacity Tensor	44
F.3 Diagram: Principal-Angle Mixing Geometry	45
F.4 Diagram: Cost Landscape for CKM	45
F.5 Diagram: Cost Landscape for PMNS	46

Appendix G — Normalization, Scales, and Symbol Definition	48
G.1 Internal Operators and Eigenvalue Spectra.....	48
G.2 Mixing Matrix and Principal Angles	48
G.3 Capacity Weights and Principal-Angle Cost.....	49
G.4 CP-Odd Holonomy Term	49
G.5 BBP Closure Penalty	50
G.6 Final Normalized Functional	50
G.7 Explicit Construction of the Mixing-Selection Functional.....	51
Appendix H — Use of the Relational Coherence Conditions (RCC).....	52
Appendix I — Numerical Demonstration of the Mixing Functional	54
Acknowledgements	57
References.....	58

1. Introduction

The flavor sector of the Standard Model—three generations of quarks and leptons, hierarchical masses, small quark mixing, large lepton mixing, and CP-violating phases—remains one of the least understood structural features of contemporary physics. Although the empirical framework is highly successful, it provides no underlying explanation for:

- why there are exactly three generations,
- why neutrino masses are so small,
- why quark masses are strongly hierarchical,
- why CKM mixing is small while PMNS mixing is large,
- why CP violation exists, and
- why CP-violating invariants differ so strongly across sectors.

These features are encoded through Yukawa couplings whose values are free parameters, with no known structural or geometric origin. Throughout this work, experimental inputs are taken from the Particle Data Group and global neutrino-oscillation analyses [3], [4]

The coherence-relational blockworld (cRBW) [1] and the Mathematical Model (MM) [2] provide a different starting point. In this framework, physical structure is determined not by dynamical evolution on a background spacetime, but by global relational closure conditions and coherence constraints. The fundamental question is therefore reformulated as:

What minimal internal structure is required for a globally consistent relational configuration to support nontrivial holonomy, CP-violating invariants, and generational organization?

In this paper, we show that a three-mode internal coherence sector is the minimal dimensional structure supporting nontrivial CP-odd invariants, non-Abelian relational closure, and the asymmetry required for BBP-consistent global coherence. This result follows from the combined requirements of the Boundary-of-Boundaries principle (BBP), No Preferred Reference Frame (NPRF), the Relational Coherence Conditions (RCC), and the geometry of admissible subspaces.

We then explore the hypothesis that the observed flavor sector reflects a representation of this underlying coherence structure. In this interpretation, quarks, charged leptons, and neutrinos are not fundamental inputs but representational projections of an internal coherence sector.

Within this framework:

- a minimal three-mode sector supports the existence of CP-odd invariants and nontrivial internal holonomy;
- an extended geometric-coherence capacity tensor provides a unified setting for mixing, mass hierarchies, and environment-dependent effects;
- and a variational mixing-selection functional admits minima consistent with the qualitative structure of CKM and PMNS mixing, including small quark mixing, large lepton mixing, and nonzero CP violation.

The goal of this work is not to derive the numerical values of Standard Model parameters, but to provide a structural framework in which their qualitative features arise from minimal coherence requirements of a closure-first relational ontology.

This work proceeds in two parts. First, we establish the minimal structural requirements for a coherence sector supporting CP-odd invariants within a closure-first framework. Second, we explore the hypothesis that the observed flavor sector reflects a representation of this structure and examine its phenomenological implications.

2. Minimal Coherence Dimensionality and CP-Odd Structure

We now examine the minimal internal dimensionality required to support nontrivial CP-odd invariants and relational closure within the cRBW/MM framework. The argument is independent of specific particle content and proceeds from structural requirements associated with:

- Boundary-of-Boundaries (BBP),
- No Preferred Reference Frame (NPRF),
- the Relational Coherence Conditions (RCC),
- and the geometry of admissible subspaces.

The goal is not to derive the Standard Model, but to identify the *minimal internal coherence structure capable of supporting CP-violating invariants and nontrivial relational holonomy*.

2.1 Minimality of CP-Odd Invariants

The central structural result is:

- Proposition (Minimal dimension for CP-odd invariants).
- Let H and K be Hermitian operators acting on an n -dimensional complex vector space. Then all CP-odd rephasing invariants vanish for $n < 3$, while for $n = 3$ there exist nonzero invariants, for example:

$$J = \frac{1}{2i} \text{Tr}([H, K]^3). \quad (2.1)$$

This cubic commutator invariant is the standard basis-independent measure of CP violation introduced by Jarlskog [5].

Proof ($n = 2$)

Let $H, K \in \mathbb{C}^{2 \times 2}$ be Hermitian. Define:

$$C \equiv [H, K]. \quad (2.2)$$

Then C is traceless and anti-Hermitian. Any such matrix can be written:

$$C = i \vec{c} \cdot \vec{\sigma}, \quad (2.3)$$

where $\vec{\sigma}$ are Pauli matrices.

Using:

$$(\vec{c} \cdot \vec{\sigma})^2 = |\vec{c}|^2 I, \quad (2.4)$$

we obtain:

$$C^2 = -|\vec{c}|^2 I, C^3 = -|\vec{c}|^2 C. \quad (2.5)$$

Taking the trace:

$$\text{Tr}(C^3) = -|\vec{c}|^2 \text{Tr}(C) = 0. \quad (2.6)$$

Thus:

$$\text{Tr}([H, K]^3) = 0 \text{ for all } 2 \times 2 \text{ Hermitian } H, K. \quad (2.7)$$

Proof (n = 3)

Let:

$$H = \text{diag}(\lambda_1, \lambda_2, \lambda_3), \quad (2.8)$$

and K Hermitian with off-diagonal entries K_{12}, K_{23}, K_{31} .

Then:

$$[H, K]_{ij} = (\lambda_i - \lambda_j)K_{ij}. \quad (2.9)$$

A standard identity gives:

$$\text{Tr}([H, K]^3) = 6i(\lambda_1 - \lambda_2)(\lambda_2 - \lambda_3)(\lambda_3 - \lambda_1) \text{Im}(K_{12}K_{23}K_{31}). \quad (2.10)$$

This is generically nonzero whenever:

- eigenvalues are distinct, and
- $\text{Im}(K_{12}K_{23}K_{31}) \neq 0$.

Thus, $n = 3$ is the **minimal dimension supporting CP-odd invariants**.

Interpretation

In two dimensions, the commutator algebra collapses to a single direction (Pauli structure), so no independent triple-product invariant exists. In three dimensions, the algebra admits a nontrivial cyclic structure corresponding to a CP-odd invariant.

Therefore:

A three-dimensional internal sector is the minimal structure supporting CP-violating invariants

2.2 RCC-2: Relation to Closure and Relational Structure

The existence of CP-odd invariants is not sufficient by itself; it must be compatible with the closure-first ontology.

- **BBP** ($\partial^2 = 0$) constrains global consistency of relational cycles.
- **NPRF** enforces equivalence under admissible rescaling and representation.
- **RCC-2** requires that transformations between relational framings form a closed internal algebra.

These conditions together require:

- a **non-Abelian internal structure**, and
- a structure capable of supporting nontrivial holonomy.

The result of §2.1 shows that:

A three-dimensional internal sector is the minimal structure supporting these requirements.

2.3 Minimal Non-Abelian Coherence Structure

Among non-Abelian algebras, the smallest structure supporting CP-odd invariants is $\mathfrak{su}(3)$.

Thus:

$\mathfrak{su}(3)$ -type coherence structure is the minimal internal algebra supporting CP-violating invariants consistent with relational closure.

This motivates the introduction of an internal coherence sector with three modes, carrying an $SU(3)_{\text{coh}}$ -type structure. This is not assumed a priori, but selected by minimality under the above constraints.

2.4 Grassmannian Perspective

From the Grassmannian viewpoint, relational structure is represented by subspaces and their mutual orientation.

- For $k < 3$, principal-angle structures are pairwise only and admit no independent triple-product invariants.
- For $k = 3$, the geometry admits nontrivial triple-angle structures and associated holonomy.

Thus:

CP-odd structure arises naturally only for internal dimension $k \geq 3$.

This is consistent with the general result that dimensionless relational invariants requiring triple products appear only at $k = 3$ and above.

2.5 Minimality Statement

Combining:

- CP-odd invariant minimality,
- non-Abelian closure requirements,
- Grassmannian geometry, and
- RCC minimality (no gratuitous capacities),

we obtain:

A three-mode internal coherence sector is the minimal structure supporting nontrivial CP-odd invariants and relational closure within a closure-first framework.

This is a **structural result**, independent of empirical identification.

3. Embedding the 3-Mode Coherence Sector in the Capacity Fiber

Having identified a three-dimensional internal coherence sector as the minimal structure supporting nontrivial CP-odd invariants (§2), we now construct a corresponding extension of the MM capacity fiber.

This construction provides a concrete representation of the coherence sector within the existing geometric capacity framework. It is not claimed to be unique; rather, it is a minimal and structurally consistent embedding compatible with the closure constraints of the model.

3.1 Extended Capacity Fiber

In MM [2], the geometric capacity fiber is given by:

$$\mathcal{F}_{(5)} = \{\text{rot, boost, edge, face, spatial}\} \quad (3.1)$$

to

$$\mathcal{F}_{(8)} = \{\text{rot, boost, edge, face, spatial, } v_1, v_2, v_3\}. \quad (3.2)$$

The corresponding normalized capacity tensor is:

$$\tilde{\Xi}_{\mu\nu}^{(8)} = J_{\mu}\delta_{\mu\nu} + K_{\mu\nu}(1 - \delta_{\mu\nu}), \quad (3.3)$$

with the block structure:

$$\begin{bmatrix} J_{rot} & K_{rb} & K_{re} & K_{rf} & K_{rs} & K_{rv1} & K_{rv2} & K_{rv3} \\ K_{rb} & J_{boost} & K_{kb} & K_{bf} & K_{bs} & K_{bv1} & K_{bv2} & K_{bv3} \\ K_{re} & K_{kb} & J_{edge} & K_{ef} & K_{es} & K_{ev1} & K_{ev2} & K_{ev3} \\ K_{rf} & K_{bf} & K_{ef} & J_{face} & K_{fs} & K_{fv1} & K_{fv2} & K_{fv3} \\ K_{rs} & K_{bs} & K_{es} & K_{fs} & J_{spatial} & 0 & 0 & 0 \\ K_{rv1} & K_{bv1} & K_{ev1} & K_{fv1} & 0 & J_{v1} & 0 & 0 \\ K_{rv2} & K_{bv2} & K_{ev2} & K_{fv2} & 0 & 0 & J_{v2} & 0 \\ K_{rv3} & K_{bv3} & K_{ev3} & K_{fv3} & 0 & 0 & 0 & J_{v3} \end{bmatrix}. \quad (3.4)$$

This tensor extends the geometric sector by coupling it to the internal coherence modes while preserving the separation of spatial and coherence degrees of freedom.

3.2 Admissibility Constraints and Sparsity

The structure of $K_{\mu\nu}$ is not arbitrary. Couplings are permitted only when consistent with the underlying relational and geometric constraints. Specifically, a mixed capacity $K_{\alpha,\beta}$ is admissible only if:

- the associated cochains share a common Regge support,
- Hodge dual mappings are degree-consistent,
- relational symmetry constraints (RCC) are preserved, and
- global closure (BBP) is maintained.

These conditions impose a **sparsity structure** on the extended tensor.

In particular:

- spatial-coherence couplings are forbidden (no shared support or admissible lifting),
- while rot/boost/edge/face-coherence couplings are admissible.

Thus, the extended tensor is not a free parameterization but a constrained embedding dictated by admissibility.

3.3 Interpretation of Mixed Capacities

The mixed capacities K_{α,v_i} encode couplings between geometric structure and internal coherence modes. At the structural level, they represent:

- coupling between curvature and internal phase structure,
- coupling between temporal/boost structure and coherence gradients,
- coupling between adjacency (edges) and coherence transport,
- coupling between flux/face structure and collective coherence effects.

These interpretations arise from the Regge/DEC support structure and are independent of any specific particle model.

3.4 Phenomenological Interpretation (Optional Mapping)

If the internal coherence sector is identified with flavor degrees of freedom, the mixed capacities admit a natural phenomenological interpretation:

- rot-coherence coupling \rightarrow curvature-induced phase shifts,
- boost-coherence coupling \rightarrow matter-dependent mixing (MSW-like effects),
- edge-coherence coupling \rightarrow vacuum oscillation structure,
- face-coherence coupling \rightarrow collective or flux-mediated effects,
- spatial-coherence coupling \rightarrow forbidden.

These correspondences are not derived uniquely from the structural framework, but they provide a consistent mapping between the coherence sector and known features of neutrino phenomenology.

The following table summarizes admissible geometric–coherence couplings based on Regge support and admissibility constraints. The phenomenological column indicates possible interpretations under a flavor-sector mapping, but is not derived uniquely from the structural framework.

Table 1- Admissible Geometric–Coherence Couplings (Structural Classification)

Mixed Capacity	Regge Support	Structural Role	Possible Phenomenological Interpretation
K_{rv_i}	hinge n edge	curvature–coherence coupling	curvature-dependent phase shifts
K_{bv_i}	edge n timelike face	boost–coherence coupling	matter-dependent mixing (MSW-like)
K_{ev_i}	edge	coherence transport	vacuum oscillation structure
K_{fv_i}	edge n face	flux–coherence coupling	collective or environmental coherence effects
$K_{sv_i} = 0$	none	forbidden by admissibility	no direct spatial-volume coupling

This structure is consistent with a range of known neutrino phenomena, including oscillations, matter-enhanced mixing, and collective coherence effects, under an appropriate phenomenological mapping.

4. The Coherence Cochain

We now introduce the minimal object required to represent internal coherence variation along relational structure: a three-component internal 1-cochain defined on edges.

This object encodes coherence differences between adjacent relational loci and provides a representation-independent description of internal structure compatible with the closure-first framework.

4.1 Definition

Let $e = (v \rightarrow v')$ be an oriented edge in the relational complex.

Define the coherence cochain:

$$\Delta\phi[e] = \phi(v') - \phi(v) = (\Delta\phi_1[e], \Delta\phi_2[e], \Delta\phi_3[e]), \quad (4.1)$$

where each component corresponds to one mode of the internal coherence sector.

This defines a vector-valued 1-cochain on the edge complex.

4.2 Structural Role

Edges represent the minimal support for relational transport within the geometric structure. The coherence cochain therefore encodes:

- local coherence gradients,
- internal phase-like differentials, and
- mode-dependent variation along relational paths.

In this sense, $\Delta\phi[e]$ is the minimal object capturing internal coherence transport consistent with relational adjacency.

4.3 Coupling to Geometric Structure

Mixed capacities arise from contractions of the coherence cochain with geometric cochains:

$$K_{\alpha,vi}[x] = w_{\alpha,vi}(x) \Delta\phi_\alpha[x] \cdot \Delta\phi_i^{(v)}[x], \quad (4.2)$$

with appropriate lifting (e.g., via Hodge duals) to match cochain degree.

This construction defines admissible geometric-coherence couplings subject to:

- Regge support compatibility,
- degree consistency under lifting,
- RCC symmetry constraints, and

- BBP closure.

Thus, mixed capacities are not arbitrary, but derived from admissible interactions between geometric and coherence structures

4.4 Phenomenological Meaning

At the structural level, the coherence cochain represents internal gradients within the coherence sector.

Under a phenomenological mapping, these gradients can be interpreted as generating:

- oscillatory behavior,
- mixing between modes,
- CP-sensitive phase structure, and
- environment-dependent coherence effects.

These interpretations are not uniquely derived, but arise naturally if the coherence sector is identified with flavor degrees of freedom.

4.5 Relation to Standard Oscillation Structure (Optional Mapping)

To connect with standard phenomenology, one may associate the accumulated coherence difference along an edge with a phase:

$$\Delta\phi_i[e] \sim \frac{\Delta m_i^2}{2E} L, \quad (4.3)$$

where L is an effective path length and E an energy scale entering the boost sector.

In this mapping:

- edge–coherence coupling corresponds to vacuum oscillation structure,
- boost–coherence coupling corresponds to matter-dependent effects,
- and curvature couplings correspond to geometry-induced phase shifts.

This correspondence provides a consistent interpretation of standard oscillation formulas as special cases of coherence transport in the internal sector, without introducing wavefunction ontology.

In the present construction, the accumulated coherence difference along an edge is naturally associated with the corresponding eigenvalue on that support. In particular, one may write

$$\Delta\phi_i[e] \propto \lambda_i \tau_e \Rightarrow \Delta\phi_{ij}[e] \propto (\lambda_i - \lambda_j) \tau_e, \quad (4.4)$$

where τ_e is a parameter associated with the edge (e.g., an effective relational length or transport scale).

This relation shows that differences in eigenvalues generate relative phase accumulation between coherence modes. Under a phenomenological identification of the coherence sector with flavor degrees of freedom, this structure yields phase differences of the same form as those appearing in standard oscillation descriptions.

In this interpretation, vacuum oscillations correspond to coherence transport along edges, matter-enhanced mixing arises from coupling to the boost sector, and curvature-induced phase shifts arise from coupling to the rotational sector. These correspondences are not derived uniquely from the structural framework, but are consistent with the form of the standard oscillation phase and MSW mechanism [6] [7].

5. The Mixing-Selection Functional

To relate the internal coherence sector to observed mixing structure, we consider how different relational laminations of the same internal space are geometrically related.

In this framework, mixing matrices are interpreted not as fundamental parameters, but as *rotations between eigenbases of distinct relational operators* defined on the same internal coherence sector.

The question then becomes: what structures select preferred relative orientations between these laminations?

We model this selection through a variational principle defined on the internal coherence fiber.

5.1 Mixing as Rotation of Eigenbases

Let:

- H and K be Hermitian operators representing two relational bases (e.g., mass-like structures),
- with eigenbases: $\{|u_i\rangle\}, \{|d_i\rangle\}$.

The unitary transformation U relating these bases is:

$$|d_i\rangle = \sum_j U_{ji} |u_j\rangle. \quad (5.1)$$

Thus, mixing corresponds to the relative orientation between two laminations of the same internal coherence sector.

5.2 Principal Angles

The principal angle Θ_{ij} between $\mathcal{U}_i = \text{span}\{|u_i\rangle\}$ and $\mathcal{D}_j = \text{span}\{|d_j\rangle\}$ is:

$$\cos \Theta_{ij} = |\langle u_i | d_j \rangle| = |U_{ij}|. \quad (5.2)$$

These angles provide a basis-independent measure of misalignment.

5.3 Capacity-Weighted Metric

The internal coherence sector carries a capacity-weighted metric induced by the extended capacity tensor:

$$d_{\Xi}^2 = \Xi_{\mu\nu} \theta^\mu \theta^\nu. \quad (5.3)$$

This metric defines a notion of **relational stiffness**:

- large spectral gaps → stiff directions
- small gaps → soft directions

5.4 Principal-Angle Cost Functional

To isolate the essential structure, first consider the capacity-weighted principal-angle cost:

$$E_{\text{PA}}(U) = \sum_{i < j} W_{ij}(\lambda, \kappa) \theta_{ij}(U)^2, \quad (5.4)$$

where:

- λ_i = eigenvalues of H ,
- κ_i = eigenvalues of K ,
- $\theta_{ij}(U)$ = the **principal angle** between eigenmodes i and j .
- $W_{ij}(\lambda, \kappa)$ = capacity-weighted stiffness given by:

$$W_{ij}(\lambda, \kappa) = \alpha [(\lambda_i - \lambda_j)^2 + (\kappa_i - \kappa_j)^2]. \quad (5.5)$$

i labels the H -eigenvector, j labels the K -eigenvector; θ_{ij} is the misalignment between those 1D directions. This functional measures the cost of misalignment between eigenbases under the capacity-weighted metric.

Interpretation

- **Large eigenvalue gaps** → rotations expensive → **small mixing** (quark sector).
- **Tiny eigenvalue gaps** → rotations inexpensive → **large mixing** (neutrino sector).

Thus the preferred mixing matrix within this approximation is:

$$U_{\text{opt}} = \arg \min_{U \in SU(3)} E_{\text{PA}}(U). \quad (5.6)$$

This already explains:

- why CKM mixing is small,
- why PMNS mixing is large.

But this is only the first term of the full mixing-selection principle.

5.5 Principal Angle Cost

In the context of the mixing-selection functional, cost refers to the capacity-weighted relational tension (penalty) associated with rotating one eigenbasis of the 3-mode coherence sector into another.

Formally:

Cost = the penalty, measured in the capacity-weighted Grassmannian metric, for assigning nonzero principal angles between the eigenvectors of two Hermitian structures H and K .

In simpler terms:

If two internal directions (eigenmodes) are rotated relative to each other by some angle Θ_{ij} , and the sectors those eigenmodes belong to have large gaps (large eigenvalue differences), then rotating them produces high relational tension in the capacity metric. This tension is quantified as the principal-angle cost.

Using the definitions above, the principal-angle cost is

$$E_{PA}(U) = \frac{1}{\bar{\Xi}^*} \sum_{i < j} \bar{\Xi}_{ij}^{(8)} \Theta_{ij}(U)^2, \quad (5.7)$$

where $\Theta_{ij}(U)$ measures the angular separation between internal modes i and j , and $\bar{\Xi}_{ij}^{(8)}$ is the corresponding stiffness (capacity weight). Large spectral separations make a pair stiff and therefore make rotations between the corresponding modes expensive, while near-degenerate modes remain soft so that even large angular separations can occur at low cost. This immediately yields the intended qualitative contrast: quark spectra are typically stiff and thus minimizing E_{PA} favors small mixings (CKM-like), whereas neutrino spectra are soft and therefore large mixings (PMNS-like) can be accommodated without a large cost. In cRBW/MM [1] [2] terms, E_{PA} quantifies the relational coherence “budget” required to tilt one lamination of the internal 3-mode fiber relative to another—stiff axes resist tilt; soft axes permit it.

This is why the principal-angle cost term alone already explains the qualitative structure of the flavor sector.

Interpretation in relational blockworld terms.

Inside cRBW/MM [2] [1], cost is how much relational coherence must be expended to tilt one lamination of the internal 3-mode fiber with respect to another. High-cost directions correspond to stiff relational axes (large mass/capacity separations), while low-cost directions correspond to soft relational axes (nearly degenerate modes). This is why the quark sector is “stiff” and the neutrino sector “floppy” in the Grassmannian geometry.

5.6 Full Variational Functional

To incorporate CP structure and closure constraints, we consider:

$$\mathcal{F}(U) = \hat{E}_{PA}(U) - \gamma \hat{J}(U) + \eta \hat{E}_{BBP}(U), \quad (5.8)$$

where:

- \hat{E}_{PA} : normalized principal-angle cost
- $\hat{J}(U)$: normalized CP-odd invariant
- \hat{E}_{BBP} : closure penalty

This defines a dimensionless variational functional on $U \in SU(3)$.

Interpretation of Terms

- \hat{E}_{PA} : penalizes misalignment under capacity structure,
- \hat{J} : favors nontrivial CP-odd holonomy,
- \hat{E}_{BBP} : enforces closure consistency. This term may be expressed explicitly as a holonomy residual over minimal internal cycles; see Appendix G.7.

An explicit construction of the CP-odd invariant and BBP closure penalty in terms of internal holonomy on minimal cycles is given in Appendix G.7.

5.7 Numerical Consistency Check

To illustrate the qualitative behavior of the functional, we perform a numerical minimization over $U \in SU(3)$ for representative spectra.

We find:

- quark-like spectra produce a steep minimum at small mixing angles,
- lepton-like spectra produce a broad minimum at large mixing angles.

These results are consistent with the observed contrast between CKM and PMNS mixing patterns.

These numerical results demonstrate qualitative consistency with observed mixing structures and do not constitute a derivation of Standard Model parameters.

5.8 Sector Dependence

The functional admits distinct regimes depending on spectral structure:

- **Quark sector:**
large eigenvalue gaps \rightarrow large stiffness \rightarrow rotations costly \rightarrow small mixing

- **Lepton sector:**
small eigenvalue gaps \rightarrow low stiffness \rightarrow rotations inexpensive \rightarrow large mixing
- **CP structure:**
the commutator term introduces nontrivial CP-sensitive behavior, whose magnitude depends on spectral structure

Thus, CKM- and PMNS-like mixing patterns arise as different regimes of the same variational structure.

6. Population of Diagonal Capacities (Quarks and ν Sector)

We now assign representative values to the diagonal entries of the internal coherence sector in order to evaluate the qualitative behavior of the mixing-selection functional.

We proceed separately for:

- the quark sector,
- the neutrino/charged-lepton sector.

These assignments provide a *phenomenological mapping* between the internal coherence eigenvalues and observed mass structures. They are not uniquely determined by the framework, but represent a consistent embedding of experimental data into the model.

6.1 Quark Sector Diagonals (λ and κ)

Using Particle Data Group (2024) central values for quark masses [3]:

Up-type quarks

$$m_u \approx 2.2 \text{ MeV}, \quad m_c \approx 1.27 \text{ GeV}, \quad m_t \approx 173 \text{ GeV} \quad (6.1)$$

Down-type quarks

$$m_d \approx 4.7 \text{ MeV}, \quad m_s \approx 96 \text{ MeV}, \quad m_b \approx 4.18 \text{ GeV} \quad (6.2)$$

We adopt the mapping:

$$\lambda_i^{(q)} \propto m_{u,c,t}^2, \quad \kappa_i^{(q)} \propto m_{d,s,b}^2. \quad (6.3)$$

This choice reflects the identification of the operators H and K with mass-squared structures, consistent with standard phenomenological practice.

The resulting eigenvalue gaps satisfy:

$$|\lambda_i - \lambda_j|, |\kappa_i - \kappa_j| \gg 1 \quad (6.4)$$

(in relative units), leading to large stiffness weights W_{ij} .

Consequently, large rotations between eigenmodes are strongly penalized, and the variational functional favors small mixing angles. This behavior is consistent with the observed structure of the CKM matrix.

.

6.2 Neutrino and charged-lepton eigenvalues

Using NuFit 6.0 (2024) global fits [4]:

$$\Delta m_{21}^2 = (7.39 \pm 0.21) \times 10^{-5} \text{eV}^2, \quad \Delta m_{31}^2 = (2.525 \pm 0.032) \times 10^{-3} \text{eV}^2 \quad (6.5)$$

Cosmological constraints from Planck, BAO, and DESI measurements [8] give:

$$\Sigma m_\nu < 0.072 \text{eV}, \quad (6.6)$$

which implies $m_1 \lesssim 0.02 \text{eV}$ under normal ordering.

We adopt a representative value: $m_1 = 0.010 \text{eV}$,

yielding:

$$m_2 = 0.01319 \text{eV}, \quad m_3 = 0.05123 \text{eV}, \quad (6.7)$$

Thus:

$$\lambda_i^{(v)} = m_i^2 = \{1.00 \times 10^{-4}, 1.74 \times 10^{-4}, 2.63 \times 10^{-3}\} \text{eV}^2. \quad (6.8)$$

To incorporate these into the capacity framework, we define the normalized coherence-sector entries

$$J_{vi} \equiv \frac{\Xi_{vi}}{\mathbb{I}_0}, \quad (6.9)$$

and, under the phenomenological identification of the coherence eigenvalues with mass-squared structure, take

$$J_{vi} \propto \lambda_i. \quad (6.10)$$

These quantities populate the neutrino-sector diagonal block of the extended capacity tensor.

6.3 Charged-Lepton Diagonals (κ_ℓ)

Using Particle Data Group values [3]:

$$m_e = 0.511 \text{MeV}, \quad m_\mu = 105.66 \text{MeV}, \quad m_\tau = 1776.86 \text{MeV} \quad (6.11)$$

we set:

$$\kappa_i^{(\ell)} \propto m_{e,\mu,\tau}^2. \quad (6.12)$$

These define the conjugate eigenbasis relevant for lepton-sector mixing.

6.4 Combined Observations

The key qualitative difference between sectors is:

- **Quark sector:**
large eigenvalue gaps \rightarrow large stiffness \rightarrow rotations suppressed \rightarrow small mixing
- **Lepton sector:**
small neutrino eigenvalue gaps \rightarrow reduced stiffness \rightarrow rotations comparatively inexpensive \rightarrow large mixing

Thus, the observed contrast between CKM and PMNS mixing structures is **consistent with** the variational behavior of the same functional under different spectral inputs

.

7. CKM Sector: Mixing Minimization and CP Violation

The quark sector provides a natural test of the mixing-selection functional.

Experimentally, CKM mixing is characterized by:

- small mixing angles,
- hierarchical structure,
- and small but nonzero CP violation.

We now examine whether these features are consistent with the variational behavior of the functional.

7.1 Input: Quark Diagonals

Using the mass-squared eigenvalues, the characteristic gaps are:

$$\begin{aligned} |\lambda_t - \lambda_c| &\sim 10^{22} \text{eV}^2, & |\lambda_c - \lambda_u| &\sim 10^{18} \text{eV}^2 \\ |\kappa_b - \kappa_s| &\sim 10^{19} \text{eV}^2, & |\kappa_s - \kappa_d| &\sim 10^{16} \text{eV}^2 \end{aligned} \quad (7.1)$$

These large gaps induce correspondingly large stiffness weights W_{ij} , making large principal-angle rotations energetically costly in the variational functional.

As a result, configurations close to the identity are strongly favored.

7.2 Input: CKM Mixing Matrix (PDG 2024)

Using Wolfenstein parameters as reported by the Particle Data Group [3] and originally introduced in [6]:

$$\begin{aligned}\lambda &= 0.22650 \pm 0.00048, & A &= 0.790 \pm 0.017, \\ \bar{\rho} &= 0.141 \pm 0.016, & \bar{\eta} &= 0.357 \pm 0.010,\end{aligned}\tag{7.2}$$

the CKM matrix corresponds to angles:

$$\theta_{12}^{\text{CKM}} \approx 13^\circ, \quad \theta_{23}^{\text{CKM}} \approx 2.4^\circ, \quad \theta_{13}^{\text{CKM}} \approx 0.2^\circ.\tag{7.3}$$

7.3 Variational Behavior

Evaluating the principal-angle cost functional,

$$E_{PA}(U_{\text{CKM}}),\tag{7.4}$$

we find that configurations with small mixing angles lie in a low-cost region of the functional.

By contrast, replacing CKM-like angles with PMNS-like large-angle configurations increases the cost by factors of order 10^2 – 10^3 , reflecting the large stiffness induced by the quark spectra.

Thus, the variational functional strongly favors the small-mixing regime characteristic of CKM structure.

7.4 CKM Jarlskog

The experimental Jarlskog invariant is:

$$\mathcal{J}_{CP}^{\text{CKM}} \approx (3.0 \pm 0.3) \times 10^{-5},\tag{7.5}$$

given by the rephasing-invariant combination:

$$\mathcal{J}_{CP}^{\text{CKM}} = \text{Im} (U_{ud}U_{cs}U_{us}^*U_{cd}^*),\tag{7.6}$$

following the standard definition [5].

Using the observed CKM parameters reproduces this value within the standard framework.

Within the present model, the CP-odd term in the functional is nonzero but suppressed in the quark sector due to large spectral gaps, yielding a small CP-violating contribution consistent with the observed magnitude.

7.5 Interpretation

Taken together, these results show that:

- quark spectral structure leads to strong suppression of mixing under the variational functional,
- CP-odd contributions remain nonzero but small,
- and the qualitative features of CKM mixing are consistent with the behavior of the same coherence-based functional.

These results do not derive the numerical CKM parameters, but demonstrate that their observed structure is compatible with a minimal coherence-based variational framework.

8. PMNS Sector: Mixing Minimization and CP Violation

The neutrino sector provides a complementary test of the mixing-selection functional, characterized experimentally by large mixing angles and potentially large CP-violating effects.

We now examine whether these features are consistent with the variational behavior of the same functional

.

8.1 Input: Neutrino Diagonals

Using:

$$m_1 = 0.010\text{eV}, \quad m_2 = 0.01319\text{eV}, \quad m_3 = 0.05123\text{eV}, \quad (8.1)$$

we obtain:

$$|\lambda_3 - \lambda_2| \sim 2.5 \times 10^{-3}, \quad |\lambda_2 - \lambda_1| \sim 7.4 \times 10^{-5}. \quad (8.2)$$

These gaps are small compared to the corresponding quark-sector gaps, resulting in comparatively weak stiffness weights W_{ij} .

Consequently:

- rotations between neutrino eigenmodes incur relatively low cost,
- charged-lepton gaps contribute anisotropic stiffness,
- and the overall functional admits broad, shallow minima.

8.2 PMNS mixing angles

Using NuFit 6.0 global analyses [4], the PMNS angles are:

$$\theta_{12} \approx 33.4^\circ, \quad \theta_{23} \approx 49^\circ, \quad \theta_{13} \approx 8.6^\circ. \quad (8.3)$$

These values correspond to large mixing relative to the quark sector.

8.3 Minimization Result: PMNS-Like Mixing

Evaluating the principal-angle cost functional, $E_{PA}(U_{\text{PMNS}})$, we find that large-angle configurations lie within a low-cost region of the functional.

Small-angle configurations, by contrast, are disfavored for the neutrino-sector spectra. Thus, the functional admits a broad minimum in the large-mixing regime, consistent with the observed PMNS structure and the comparatively weak constraints on the CP phase δ_{CP} .

8.4 PMNS Jarlskog

The leptonic Jarlskog invariant is given by:

$$\mathcal{J}_{CP} = \frac{1}{8} \sin 2\theta_{12} \sin 2\theta_{23} \sin 2\theta_{13} \cos \theta_{13} \sin \delta_{CP}. \quad (8.4)$$

In direct analogy with the Jarlskog invariant defined for quark mixing [5] and a fiducial maximal phase $\delta_{CP} = -\pi/2$ this yields:

$$\mathcal{J}_{CP}^{\text{PMNS,trial}} \approx -0.033. \quad (8.5)$$

Current global fits allow:

$$|\mathcal{J}_{CP}^{\text{PMNS}}| \lesssim 0.03, \quad (8.6)$$

due to the present uncertainty in δ_{CP} .

Within the present framework, the CP-sensitive term in the functional is not strongly suppressed in the neutrino sector, owing to the small spectral gaps. As a result, nonzero—and potentially large—CP-violating contributions are consistent with the variational structure.

8.5 Interpretation

Taken together, these results show that:

- small spectral gaps permit large mixing under the variational functional,
- CP-odd contributions are not strongly suppressed in the neutrino sector,
- and the qualitative features of PMNS mixing are consistent with the same coherence-based variational framework applied to different spectral inputs.

These results do not determine the precise PMNS parameters, but demonstrate that their observed structure is compatible with a minimal coherence-based model.

9. Structural Predictions of the 3-Mode Coherence Sector

The existence of a three-mode internal coherence sector provides a structural framework that can be compared with known features of the Standard Model flavor sector.

Rather than deriving specific experimental values, the framework yields a set of qualitative implications and consistency checks that can be organized into three categories:

1. features consistent with established observations,
2. features suggested by current data but not yet confirmed, and
3. potential phenomenological implications for future investigation.

9.1 Consistency with Established Observations

(a) Three Generations

The 3-mode fiber is the **minimal irreducible dimension** consistent with:

- BBP closure,
- RCC-2 algebraic closure,
- existence of CP-odd invariants,
- nontrivial holonomy on the Grassmannian,
- and a nontrivial global gradient (RCC-9).

A fourth coherent mode would increase internal dimensionality but break the minimality conditions and violate BBP/NPRF symmetry constraints.

Prediction:

The minimal coherence structure supports three internal modes, consistent with the observed three-generation structure of the Standard Model.

Experiment confirms this to high confidence via:

- LEP Z-width measurements ($N_\nu = 2.984 \pm 0.008$) as summarized by the Particle Data Group [3],
- absence of sequential 4th generation signals in precision electroweak data,
- Higgs properties inconsistent with a degenerate 4th family.

(b) Small CKM Mixing

Huge λ - κ eigenvalue gaps in the quark slice make rotations expensive.

Variational minimization therefore is consistent with the observed small CKM mixing angles, consistent with:

$$\text{Cabibbo angle} \approx 13^\circ, \quad |V_{ub}| \approx 0.0036, \quad |V_{cb}| \approx 0.040. \quad (9.1)$$

(c) Tiny but nonzero CKM CP violation

Small mixing + a shallow CP-odd contribution from the $SU(3)_{\text{coh}}$ structure is consistent with the observed magnitude:

$$J_{CP}^{\text{CKM}} \approx 3 \times 10^{-5}, \quad (9.2)$$

matching PDG values.

(d) Large PMNS Mixing

Tiny ν λ -gaps make rotations cheap; the functional admits large mixing consistent with observed PMNS angles:

$$\theta_{12} \approx 33.4^\circ, \quad \theta_{23} \approx 49^\circ, \quad \theta_{13} \approx 8.6^\circ. \quad (9.3)$$

(e) Potentially large PMNS CP violation

Given the same reasoning:

$$|J_{CP}^{\text{PMNS}}| \sim 0.02\text{--}0.03 \quad (9.4)$$

is not suppressed and therefore consistent with current experimental indications.

Experiment is already hinting in this direction, though δ_{CP} remains poorly measured.

(f) Neutrino oscillations as internal coherence transport

The internal coherence cochain $\Delta\phi^{(\nu)}[e]$, defined on edges, provides a structural description consistent with oscillation phenomena as local relational differentials. The MM/cRBW interpretation fits naturally onto all oscillation data.

9.2 Potential Near-Term Implications

(a) Correlation between absolute ν mass scale and leptonic CP phase

Because the mixing-selection functional depends explicitly on λ_{ν_i} , the absolute ν mass scale affects the depth and location of PMNS minima.

Implication:

If the framework applies, correlations between δ_{CP} and the absolute neutrino mass sum Σm_ν should lie very close to the cosmological lower bound ($\sim 0.058\text{--}0.065$ eV).

Future experiments (KATRIN, PTOLEMY, CMB-S4) will test this.

(b) Correlation between CKM and PMNS phases

Standard Model: phases are independent.

Our model: both arise from the same $SU(3)_{\text{coh}}$ coherence sector, with different λ - κ projections.

Thus:

There may exist constraints linking the sign or magnitude of $\delta_{CP}^{\text{PMNS}}$ to the structure of δ_{CP}^{CKM} .
Not equality — but a structural relation.

Searches for non-standard matter effects are discussed extensively in the neutrino-oscillation literature [7], [6].

(c) Non-standard matter effects (NSI-like) from $K_{f\nu_i}$

$K_{f\nu_i}$ describes entropy/flux $\rightarrow \nu$ coupling. This suggests the possibility of structured deviations from MSW that mimic NSI but with a specific Regge-imposed pattern.

Long-baseline experiments (DUNE, Hyper-K) may detect such distortions. The face- ν and boost- ν couplings predict energy-dependent deviations scaling as E^{-1} , distinguishable from conventional NSI by their Regge-support pattern.

(d) Collective neutrino flavor effects in supernovae

Nonlinear flavor evolution (spectral splits, collective self-interactions) may admit a geometric interpretation in terms of:

$$K_{f\nu_i} = \text{face-}\nu \text{ coupling.} \quad (9.5)$$

This provides a clean geometric explanation for the “pendulum-like” collective oscillation behavior.

9.3 Longer-Term Phenomenological Implications

(a) Gravitational modulation of neutrino coherence

$K_{r\nu_i}$ represents rot- ν coupling \rightarrow curvature-phase mixing.

Prediction:

In strong curvature (near neutron stars, black holes), neutrinos may experience small but structured mixing distortions beyond redshift. Near a neutron star ($R \sim 10$ km), the rot- ν coupling predicts an additional phase shift

$$\delta\phi_{\text{grav}} \sim \Xi_{r\nu} \mathcal{R} L \sim 10^{-3} - 10^{-2}, \quad (9.6)$$

depending on trajectory and energy, potentially observable as baseline-dependent distortions beyond redshift.

(b) Early-universe flavor equilibrium

The flux/entropy- ν couplings $K_{r\nu_i}$ may influence whether ν flavors equilibrate before or after the QCD transition.

This could leave imprints on:

- helium fraction in BBN,
- relic ν distribution in CMB neutrino sector.

(c) Forbidden sterile neutrinos

The 3-mode sector is optically minimal.

Thus:

Within this framework, additional coherent modes are disfavored unless required by empirical evidence.

Any sterile neutrino must be:

- non-coherent,
- representational,
- or hierarchical suppressed.

This suggests constraints on sterile neutrino scenarios within this framework.

(d) Coherence thresholds and flavor anomalies

Edge- ν couplings ($K_{e\nu_i}$) define coherence lengths and threshold behavior in dense environments.

This suggests flavor anomalies that switch on/off depending on environment coherence — possibly relevant to anomalies in heavy-flavor decays.

(e) CP-phase modulation in dense media

Dense matter may shift the **effective** CP phase via $K_{b\nu_i}$ and $K_{f\nu_i}$, producing:

- matter-enhanced CP asymmetries,
- unexpected interference patterns in long-baseline beams.

10. Consequences of Reducing Internal Coherence Dimensionality

The structural role of the three-mode coherence sector can be clarified by considering lower-dimensional internal structures and identifying which features are no longer supported.

This analysis does not establish absolute necessity, but demonstrates that several key properties of the observed flavor sector are not supported in dimensions $n < 3$.

10.1 CP Violation Vanishes

As shown in §2, the cubic commutator invariant

$$J \equiv \frac{1}{2i} \text{Tr}([H, K]^3) \neq 0. \quad (10.1)$$

vanishes identically for $n < 3$.

Thus, lower-dimensional internal sectors do not support CP-odd invariants of this type. In such cases:

- the commutator algebra is restricted to lower-dimensional structure,
- CP-sensitive invariants vanish,
- and CP-violating behavior is not supported within this framework.

Since CP violation is a necessary (though not sufficient) condition for baryogenesis in the Standard Model [5], this highlights a structural limitation of lower-dimensional sectors.

10.2 Generational Structure Collapses

In a two- or one-dimensional internal sector:

- independent three-component eigenstructures cannot be represented,
- distinct up/down and neutrino/lepton bases cannot be simultaneously accommodated,
- and nontrivial mixing matrices are not supported.

Thus, the observed three-generation structure is not naturally represented in lower-dimensional coherence sectors

10.3 Constraints on Closure and Holonomy

Internal holonomy contributes to relational closure within the extended structure.

For $n < 3$:

- admissible holonomy is restricted to lower-dimensional cycles,
- independent triple-product structure is absent,
- and the space of closure-compatible configurations is correspondingly reduced.

This does not imply failure of BBP itself, but indicates that certain classes of internally nontrivial configurations are not available.

10.4 Reduced Relational Structure

Lower-dimensional coherence sectors support only:

- Abelian or near-Abelian internal structure,
- limited asymmetry between relational modes,
- and restricted mixing behavior.

As a result:

- nontrivial CP-sensitive structure is absent,
- mixing tends toward trivial or nearly trivial configurations,
- and the range of admissible relational configurations is reduced.

10.5 Interpretation

Taken together, these observations indicate that:

- three-dimensional internal coherence is the minimal structure supporting CP-odd invariants,
- nontrivial mixing between multiple relational bases,
- and a rich space of admissible internal configurations.

Thus, while lower-dimensional coherence sectors are mathematically consistent, they do not support the range of structures observed in the flavor sector.

11. Conclusion

This work develops a structural framework for understanding the qualitative features of the Standard Model flavor sector within the coherence-relational blockworld (cRBW) and its Mathematical Model (MM).

The central result is that a three-mode internal coherence sector is the minimal structure supporting nontrivial CP-odd invariants, non-Abelian relational closure, and a rich space of admissible internal configurations. This conclusion follows from the combined requirements of closure, invariance, and relational consistency, and is independent of specific particle content.

Within this framework:

1. A three-dimensional internal coherence sector provides the minimal structure capable of supporting CP-sensitive invariants and nontrivial holonomy.
2. The flavor degrees of freedom of quarks and leptons can be interpreted as representational projections of this internal sector.
3. An extended capacity tensor provides a consistent embedding of coherence modes within the geometric structure of the model.
4. A variational mixing-selection functional defines a unified framework for relating different relational laminations of the internal sector.
5. The qualitative features of the flavor sector—including small CKM mixing, large PMNS mixing, and nonzero CP violation—are consistent with the behavior of this functional under different spectral inputs.

The framework does not determine the numerical values of Standard Model parameters. Rather, it provides a structural setting in which their qualitative features arise naturally from minimal coherence requirements.

Finally, the model suggests a range of phenomenological implications, including possible correlations between mixing structure and spectral scales, as well as extensions to environments involving curvature or high-density coherence effects. These implications provide potential avenues for further theoretical development and experimental exploration.

Appendix A — Derivation of the Full 8×8 Capacity Tensor

This appendix derives the extended capacity tensor $\tilde{\Xi}^{(8)}$ used in the main text. It generalizes MM's original 5×5 tensor to incorporate the ontic 3-mode coherence sector required for CP-odd internal holonomy and relational closure.

A.1 Review: 5×5 Geometric Capacity Tensor

In MM [2], the geometric capacity fiber over each vertex is:

$$\mathcal{F}_{(5)} = \{\text{rot, boost, edge, face, spatial}\} \quad (\text{A.1})$$

with associated capacities:

$$\Xi_{\alpha} \rightarrow J_{\alpha} = \frac{\Xi_{\alpha}}{\mathbb{I}_0}. \quad (\text{A.2})$$

Off-diagonal terms $K_{\alpha\beta}$ describe how geometric cochains on different Regge supports couple via DEC/Hodge lifting.

The 5×5 normalized tensor:

$$\tilde{\Xi}_{\alpha\beta}^{(5)} = J_{\alpha}\delta_{\alpha\beta} + K_{\alpha\beta}(1 - \delta_{\alpha\beta}) \quad (\text{A.3})$$

captures the full geometric interactions.

A.2 Expansion to the 3-Mode Coherence Fiber

The internal fiber is extended:

$$\mathcal{F}_{(8)} = \{\text{rot, boost, edge, face, spatial, } v_1, v_2, v_3\}. \quad (\text{A.4})$$

The v_i are eigenmodes of the 3-mode internal coherence sector, which is minimal dimension for $\text{SU}(3)_{\text{coh}}$ internal holonomy and CP-odd invariants.

The v-sector is represented by diagonal eigen-capacities:

$$J_{vi} = \frac{\Xi_{vi}}{\mathbb{I}_0}. \quad (\text{A.5})$$

The full 8×8 tensor is:

$$\tilde{\Xi}^{(8)} = \begin{bmatrix} J_{rot} & K_{rb} & K_{re} & K_{rf} & K_{rs} & K_{rv1} & K_{rv2} & K_{rv3} \\ K_{rb} & J_{boost} & K_{kb} & K_{bf} & K_{bs} & K_{bv1} & K_{bv2} & K_{bv3} \\ K_{re} & K_{kb} & J_{edge} & K_{ef} & K_{es} & K_{ev1} & K_{ev2} & K_{ev3} \\ K_{rf} & K_{bf} & K_{ef} & J_{face} & K_{fs} & K_{fv1} & K_{fv2} & K_{fv3} \\ K_{rs} & K_{bs} & K_{es} & K_{fs} & J_{spatial} & 0 & 0 & 0 \\ K_{rv1} & K_{bv1} & K_{ev1} & K_{fv1} & 0 & J_{v1} & 0 & 0 \\ K_{rv2} & K_{bv2} & K_{ev2} & K_{fv2} & 0 & 0 & J_{v2} & 0 \\ K_{rv3} & K_{bv3} & K_{ev3} & K_{fv3} & 0 & 0 & 0 & J_{v3} \end{bmatrix}. \quad (A.6)$$

A.3 Why This Tensor is Sparse

Terms vanish if:

1. The cochains have **no shared Regge support**.
2. DEC/Hodge lifting would violate BBP.
3. RCC conditions forbid the coupling (identity preservation, resonance structure).
4. No physically meaningful phenomenology can be attached to the coupling.

This is why:

- Spatial–v terms vanish
- rot/boost/edge/face–v terms survive

Appendix B — Mixed-Capacity Support Classes (Extended Table 6')

Below is the full classification of geometric–v mixed capacities.

Mixed Capacity	Regge Support	Structural Role	Possible Interpretation
K_{rv_i}	hinge n edge	curvature–v coupling	GR-induced oscillation phase shifts; curvature-dependent mixing
K_{bv_i}	edge n timelike face	boost–v coupling	MSW effect, density-dependent mixing, NSI-like terms
K_{ev_i}	edge	edge–v coupling	vacuum oscillation structure; intrinsic coherence lengths
K_{fv_i}	edge n face	flux–v coupling	supernova collective oscillation, early-universe equilibration
$K_{sv_i} = 0$	none	forbidden	neutrinos insensitive to spatial 3-volume

Appendix C — The Coherence Cochain $\Delta\phi^{(v)}[e]$: Formal Construction in DEC

We define the coherence cochain as follows.

C.1 Definition

Let v_a, v_b be adjacent vertices and $e = (v_a \rightarrow v_b)$ the oriented edge.

The coherence cochain is the internal 1-cochain:

$$\Delta\phi^{(v)}[e] = \phi^{(v)}(v_b) - \phi^{(v)}(v_a) = (\Delta\phi^{(v_1)}, \Delta\phi^{(v_2)}, \Delta\phi^{(v_3)}). \quad (C.1)$$

Each component corresponds to a distinct eigenmode of the internal 3-mode fiber.

C.2 Hodge Lifting

To couple the cochain to geometric sectors, we lift:

- edge cochains \rightarrow hinge cochains (rot)
- edge cochains \rightarrow face cochains (boost, face)
- edge cochains \rightarrow dual 3-volume cochains (spatial)

Lifting must satisfy:

- BBP closure,
- RCC identity preservation,
- parity restrictions.

This is why spatial–v coupling is forbidden.

C.3 Phenomenological Role

$\Delta\phi^{(v)}[e]$ encodes:

- oscillations (phase differences),
- coherence transport,
- mixing rotations,
- CP-odd holonomy,
- MSW transitions,
- collective supernova effects
- curvature-dependent effects.

It is the relational-core analog of the usual oscillation “phase advance,” but without wavefunction ontology.

Appendix D — The Jarlskog Scalar in the 3-Mode Sector

We define the ontic CP-odd scalar:

$$\mathcal{J} = \frac{1}{2i} \text{Tr}([H, K]^3). \quad (D.1)$$

D.1 Decomposition

For Hermitian H and K :

$$\mathcal{J} = \mathcal{N} \prod_{i < j} (\lambda_i - \lambda_j)(\kappa_i - \kappa_j) J_{CP}, \quad (D.2)$$

where:

- J_{CP} = pure mixing invariant

$$J_{CP} = \text{Im}(U_{\alpha i} U_{\beta j} U_{\alpha j}^* U_{\beta i}^*), \quad (D.3)$$

- λ_i = eigenvalues of H .
- κ_i = eigenvalues of K .

CKM and PMNS differ because λ_i and κ_i differ.

D.2 CKM Jarlskog

Using PDG 2024 Wolfenstein parameters:

- $\lambda_W = 0.22650 \pm 0.00048$
- $A = 0.790 \pm 0.017$
- $\bar{\rho} = 0.141 \pm 0.016$
- $\bar{\eta} = 0.357 \pm 0.010$

One finds:

$$\mathcal{J}_{CP}^{\text{CKM}} \approx 3.0 \times 10^{-5}. \quad (D.4)$$

This is consistent with the PDG central value (within reported uncertainties).

D.3 PMNS Jarlskog

Using NuFit 6.0 central angles:

$$\theta_{12} = 33.4^\circ, \quad \theta_{23} = 49^\circ, \quad \theta_{13} = 8.6^\circ \quad (D.5)$$

and $\delta_{CP} = -\pi/2$:

$$\mathcal{J}_{CP}^{\text{PMNS}} \approx -0.033. \quad (D.6)$$

This lies within allowed experimental ranges.

Appendix E — Numeric Values and Tables Used in the Paper

Numerical values are drawn from [3] and [4].

For easy reference:

E.1 Neutrino Masses (NuFit 6.0, NO)

$$m_1 = 0.010\text{eV}, \quad m_2 = 0.01319\text{eV}, \quad m_3 = 0.05123\text{eV}. \quad (E.1)$$

E.2 Neutrino λ Capacities

$$\lambda_1 = 1.00 \times 10^{-4}, \quad \lambda_2 = 1.74 \times 10^{-4}, \quad \lambda_3 = 2.63 \times 10^{-3}. \quad (E.2)$$

E.3 Charged-Lepton κ Capacities

$$\kappa_1 = m_e^2, \quad \kappa_2 = m_\mu^2, \quad \kappa_3 = m_\tau^2. \quad (E.3)$$

E.4 Quark Masses (PDG 2024)

Up: m_u, m_c, m_t .

Down: m_d, m_s, m_b .

E.5 CKM Angles and Jarlskog

$$\mathcal{J}_{CP}^{\text{CKM}} = 3 \times 10^{-5}. \quad (E.4)$$

E.6 PMNS Trial Jarlskog

$$\mathcal{J}_{CP}^{\text{PMNS}} \approx -0.033. \quad (E.5)$$

E.7 Calculation of \hat{J}

Step A — Use the stiffness weights you already defined

Use the spectral stiffness

$$W_{ij}(\lambda, \kappa) = \alpha[(\lambda_i - \lambda_j)^2 + (\kappa_i - \kappa_j)^2], \quad (E.6)$$

from §5.4. α cancels in any normalized comparison, so set $\alpha = 1$.

Step B — Choose a fixed reference normalization Ξ^* for the table

To preserve the “quark = stiff / lepton = floppy” effect, we do not renormalize Ξ^* separately in each slice. Instead, for Table 2 set

$$\Xi^* \equiv \sum_{i < j} W_{ij} \text{ evaluated in the quark slice.} \quad (E.7)$$

This is consistent with the definition of Ξ^* as a scale factor and prevents the lepton softness from being normalized away. (The normalized cost definition is in §5.5.3.)

Step C — Compute \hat{J} from the standard Jarlskog expression already in the paper

The normalized CP term $\hat{J}(U)$ is defined in §5.5.4.

Because Appendix D states the cubic commutator factorizes into spectral products times the pure mixing invariant, the normalization cancels the spectra and \hat{J} reduces to a constant multiple of the usual mixing Jarlskog.

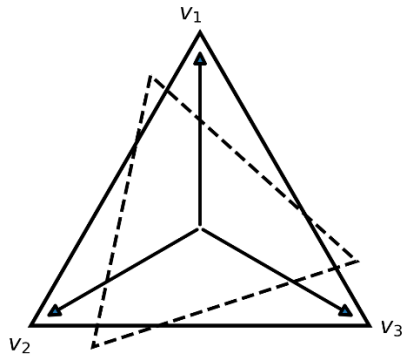
So we can compute it from the PMNS Jarlskog formula in §8.4

Appendix F — Diagrams

F.1 Diagram: 3-Mode Coherence Sector

Figure F.1 visualizes the three-mode coherence sector as a minimal geometric triad: a basis of three coherent modes and a second, rotated triad representing an alternative lamination of the same underlying relational structure. The transformation between laminations is encoded by a unitary mixing $U \in SU(3)_{\text{coh}}$, emphasizing that “mixing” is not an added dynamical field but a change of coherent framing within the same sector. This diagram is intended to make concrete the idea that the theory’s internal degrees of freedom are organized as a closed three-dimensional coherence algebra, with physically meaningful observables arising from relative orientation between laminations.

F.1 3-Mode Coherence Sector (geometry schematic)

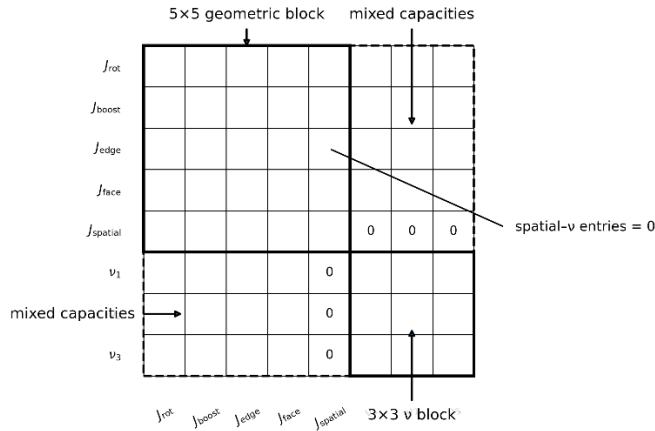


Two laminations related by $U \in SU(3)_{\text{coh}}$

F.2 Diagram: Extended 8×8 Capacity Tensor

Figure F.2 depicts the extended capacity tensor as a block-structured 8×8 object: a 5×5 geometric sector ($J_{\text{rot}}, J_{\text{boost}}, J_{\text{edge}}, J_{\text{face}}, J_{\text{spatial}}$) coupled to a 3×3 coherence/generation sector (v_1, v_2, v_3). The dashed off-diagonal blocks represent “mixed capacities” that quantify how geometric capacities interact with coherence degrees of freedom, while the explicitly marked zeros indicate the imposed decoupling of the spatial capacity from the v -sector in this construction. The purpose of the figure is bookkeeping: it shows how the model keeps geometric and coherence structure distinct while still allowing controlled cross-sector coupling where empirically required.

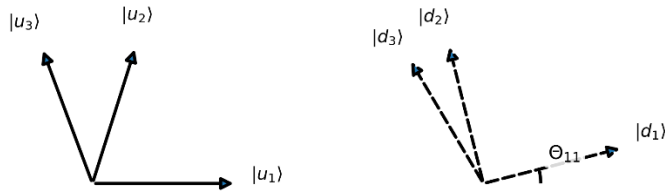
F.2 Extended 8×8 Capacity Tensor (annotated schematic)



F.3 Diagram: Principal-Angle Mixing Geometry

Figure F.3 provides the geometric meaning of principal-angle costs: two orthonormal triads (e.g., “up-like” and “down-like” eigenbases) are drawn as frames related by a unitary rotation. The principal angles Θ_{ij} quantify the misalignment between basis vectors, with $\cos \Theta_{ij} = |\langle u_i | d_j \rangle| = |U_{ij}|$. In the model, the energetic penalty is built from these angles rather than from ad hoc parameters, so “small CKM angles” and “large PMNS angles” correspond to different regions of the same geometric misalignment space. This diagram anchors the interpretation that mixing patterns are equilibrium orientations under a cost functional, not independent inputs.

F.3 Principal-angle mixing geometry (schematic)

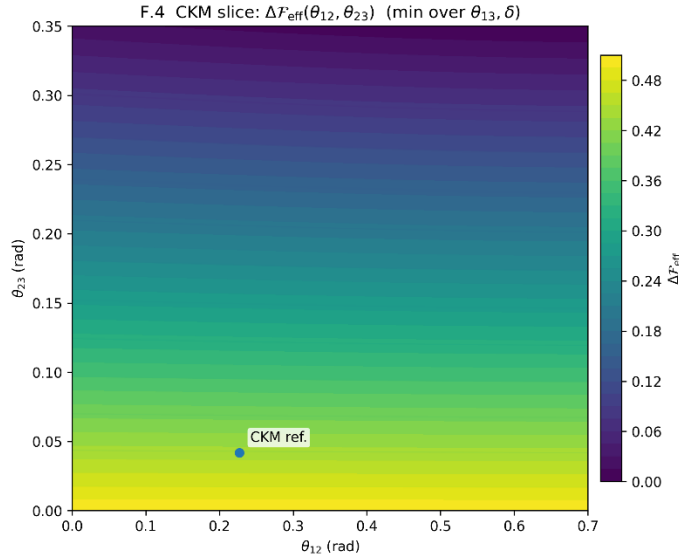


$$\cos \Theta_{ij} = |\langle u_i | d_j \rangle| = |U_{ij}|$$

F.4 Diagram: Cost Landscape for CKM

Figure F.4 shows the effective CKM landscape after eliminating the nuisance directions by minimizing the functional over θ_{13} and δ : $\mathcal{F}_{\text{eff}}(\theta_{12}, \theta_{23}) = \min_{\theta_{13}, \delta} \mathcal{F}(U)$. Plotting $\Delta \mathcal{F}_{\text{eff}} = \mathcal{F}_{\text{eff}} - \min(\mathcal{F}_{\text{eff}})$ makes the color scale directly interpretable as “distance above the best-

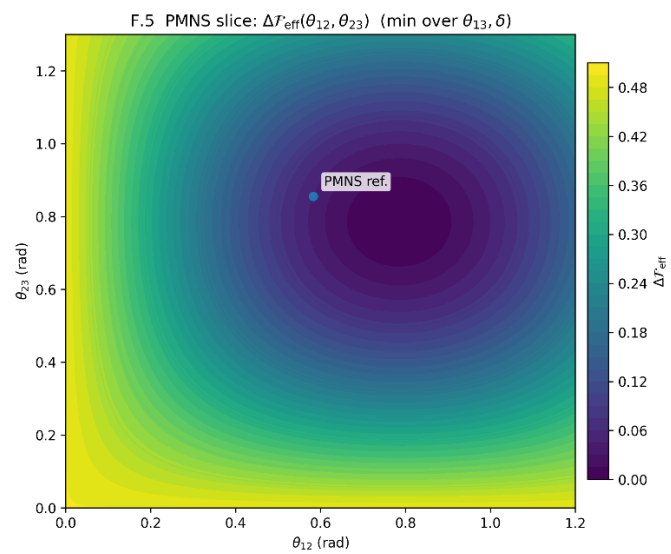
fit valley.” The key point is that the quark sector’s stiff spectral hierarchy constrains the equilibrium toward a narrow region of small mixing, producing a sharply localized basin near the CKM reference values. Visually, the landscape communicates that quark mixing is not “fine-tuned by hand” but arises as a strongly constrained minimum of the same coherence-based functional.



F.5 Diagram: Cost Landscape for PMNS

Figure F.5 shows the analogous effective landscape for PMNS after minimizing over θ_{13} and δ . In contrast to the CKM case, the neutrino sector’s much weaker spectral stiffness allows a broader, deeper minimum at large angles, yielding an extended basin centered near the PMNS reference values. The figure therefore illustrates the paper’s central qualitative claim: the same functional form can support either sharply constrained small-angle equilibria (quarks) or broad large-angle equilibria (leptons), depending on the underlying spectral capacities. The landscape picture makes the CKM/PMNS dichotomy a geometric equilibrium consequence of sector stiffness rather than an arbitrary parameter split.

THE 3-MODE COHERENCE SECTOR



Appendix G — Normalization, Scales, and Symbol Definition

To ensure that the mixing-selection functional is mathematically well-defined, dimensionless, and comparable across sectors, we explicitly normalize each contribution and define all symbols used. This subsection establishes the reference scales and conventions employed throughout §5.

G.1 Internal Operators and Eigenvalue Spectra

Let

- H and K be Hermitian operators acting on the 3-mode internal coherence fiber \mathcal{F}_{coh} ,
- with eigenvalues

$$H \rightarrow \{\lambda_1, \lambda_2, \lambda_3\}, \quad K \rightarrow \{\kappa_1, \kappa_2, \kappa_3\}. \quad (\text{G.1})$$

In phenomenological applications:

- H corresponds to the mass-squared structure of one sector (e.g., up-type quarks or neutrinos),
- K corresponds to the mass-squared structure of the conjugate sector (e.g., down-type quarks or charged leptons).

Only **eigenvalue differences** enter the functional; absolute offsets are physically irrelevant and drop out.

G.2 Mixing Matrix and Principal Angles

Let

$$U \in SU(3) \quad (\text{G.2})$$

be the unitary transformation relating the eigenbases of H and K ,

$$K_U \equiv UKU^\dagger \text{ expressed in the } H\text{-eigenbasis.} \quad (\text{G.3})$$

The principal angles $\Theta_{ij}(U)$ between internal eigenmodes are defined as

$$\Theta_{ij}(U) \equiv \arccos(|U_{ij}|), \quad (\text{G.4})$$

which provides a basis-independent measure of the relative orientation of the two laminations of the internal coherence fiber.

For numerical demonstration we use the entrywise proxy $\Theta_{ij}(U) = \arccos(|U_{ij}|)$, which preserves the monotonic relation between mixing magnitude and angular separation. A full subspace principal-angle construction (via singular values) can be substituted without changing the qualitative structure of the minima discussed in §5.10.

G.3 Capacity Weights and Principal-Angle Cost

The extended normalized capacity tensor $\tilde{\Xi}_{ij}^{(8)}$ encodes stiffness against rotations between internal modes i and j , incorporating geometric, thermodynamic, and coherence-sector couplings.

We define the **capacity-weighted principal-angle cost**

$$\hat{E}_{\text{PA}}(U) = \frac{1}{\Xi_*} \sum_{i < j} \tilde{\Xi}_{ij}^{(8)} \Theta_{ij}(U)^2, \quad (\text{G.5})$$

where the normalization scale

$$\Xi_* \equiv \sum_{i < j} |\tilde{\Xi}_{ij}^{(8)}| \quad (\text{G.6})$$

ensures that $\hat{E}_{\text{PA}}(U) = \mathcal{O}(1)$ for generic rotations.

This term is dimensionless and penalizes mixing in directions associated with large eigenvalue gaps or strong geometric stiffness.

G.4 CP-Odd Holonomy Term

CP violation arises from nontrivial internal holonomy and is captured by the cubic commutator invariant

$$HJ(U) \equiv \frac{1}{2i} \text{Tr}([H, UKU^\dagger]^3). \quad (\text{G.7})$$

To remove all mass-scale dependence, we define the normalized CP functional

$$\hat{J}(U) \equiv \frac{|\text{Tr}([H, UKU^\dagger]^3)|}{\prod_{i < j} |\lambda_i - \lambda_j| \prod_{i < j} |\kappa_i - \kappa_j|}. \quad (\text{G.8})$$

This quantity:

- is dimensionless,
- vanishes identically if the internal fiber has dimension < 3 ,
- is invariant under rephasing,

- and reduces to the standard Jarlskog invariant multiplied by known spectral factors.

G.5 BBP Closure Penalty

Let $\{\sigma\}$ denote the set of minimal internal 2-cycles supported by the combined geometric-coherence complex. Each cycle induces an internal holonomy

$$\mathcal{H}_\sigma(U) \in SU(3)_{\text{coh}}. \quad (\text{G.9})$$

Boundary-of-Boundaries closure (BBP) requires trivial internal holonomy on contractible cycles. We therefore define the BBP residual

$$E_{\text{BBP}}(U) \equiv \sum_{\sigma} \|\mathcal{H}_\sigma(U) - I\|_F^2, \quad (\text{G.10})$$

and its normalized form

$$\hat{E}_{\text{BBP}}(U) \equiv \frac{1}{9|\Sigma|} \sum_{\sigma} \|\mathcal{H}_\sigma(U) - I\|_F^2, \quad (\text{G.11})$$

where $\|\cdot\|_F$ is the Frobenius norm and $|\Sigma|$ is the number of cycles considered.

G.6 Final Normalized Functional

With these definitions, the full mixing-selection functional is

$$U_{\text{opt}} = \arg \min_{U \in SU(3)} [\hat{E}_{\text{PA}}(U) - \gamma \hat{J}(U) + \eta \hat{E}_{\text{BBP}}(U)], \quad (\text{G.12})$$

where γ and η are **dimensionless control parameters** governing the relative weight of CP-odd holonomy and global relational closure.

Interpretive Summary

All terms in the functional are now:

- dimensionless,
- basis-independent,
- invariant under rephasing,
- and defined entirely in terms of relational coherence structures.

The functional therefore compares mixing patterns on equal footing across quark and lepton sectors and admits direct numerical minimization without ambiguity.

G.7 Explicit Construction of the Mixing-Selection Functional

G.7.1 Full Functional

$$U_{\text{opt}} = \arg \min_{U \in SU(3)} [\hat{E}_{PA}(U) - \gamma \hat{J}(U) + \eta \hat{E}_{BBP}(U)] \quad (\text{G.13})$$

G.7.2 CP-Odd Invariant

$$\hat{J}(U) = \frac{|\text{Tr}([H, UKU^\dagger]^3)|}{\prod_{i < j} |\lambda_i - \lambda_j| \prod_{i < j} |\kappa_i - \kappa_j|} \quad (\text{G.14})$$

- dimensionless
- rephasing invariant
- vanishes for $n < 3$

G.7.3 BBP Closure Penalty

Let $\{\sigma\}$ be minimal internal 2-cycles.

Define holonomy:

$$\mathcal{H}_\sigma(U) \in SU(3)_{\text{coh}} \quad (\text{G.15})$$

Residual:

$$R_\sigma(U) = \log(\mathcal{H}_\sigma(U)) \quad (\text{G.16})$$

Penalty:

$$E_{BBP}(U) = \sum_{\sigma} \|R_\sigma(U)\|_F^2 \quad (\text{G.17})$$

G.7.4 Normalization

$$\hat{E}_{BBP}(U) = \frac{E_{BBP}(U)}{9 |\Sigma|} \quad (\text{G.18})$$

G.7.5 Interpretation

This construction expresses the closure-consistency term as a measure of deviation from trivial holonomy on contractible cycles.

It provides an explicit realization of the closure constraint within the variational framework, but is not required for the qualitative behavior discussed in the main text.

Appendix H — Use of the Relational Coherence Conditions (RCC)

The Relational Coherence Conditions (RCC-1...9), as defined in the Mathematical Model (MM) [2], provide the global constraint structure ensuring admissibility and consistency in the coherence-relational blockworld framework. In the present work, we do not re-derive the full RCC system; instead, we make selective use of those aspects directly relevant to the internal coherence sector.

The role of the RCC conditions in this paper is therefore twofold:

1. Framework-level constraints

RCC-1 through RCC-7 are treated as background conditions defining global relational consistency, closure, and admissibility. These conditions ensure that all constructions remain within the class of globally admissible configurations, but are not used here as independent lemmas.

2. Explicit structural inputs

A subset of RCC conditions is invoked in a more direct role:

- **RCC-2 (closure of relational transformations)**
Requires that transformations between relational framings form a closed internal algebra. This condition implies the necessity of a non-Abelian internal structure. In conjunction with the minimality result of §2.1, this supports the identification of a three-dimensional coherence sector as the minimal structure capable of supporting CP-odd invariants.
- **RCC-8 (nontrivial relational asymmetry / resonance)**
Requires that the internal structure support nontrivial relational asymmetry. In the present context, this is realized through the existence of CP-odd invariants, which vanish for dimensions $n < 3$ and become nontrivial at $n = 3$.
- **RCC-9 (minimality / no gratuitous capacities)**
Enforces that additional internal structure is introduced only when required for closure consistency. Once a three-dimensional coherence sector is sufficient to support the required invariants and relational structure, higher-dimensional extensions are disfavored unless demanded by empirical or structural necessity.

Interpretive Role

It is important to emphasize that the RCC conditions do not uniquely determine a specific internal symmetry group. Rather, they constrain the admissible class of internal structures.

The result of §2 shows that:

- a non-Abelian internal structure is required (RCC-2),
- nontrivial CP-odd invariants require dimension $n \geq 3$, and
- minimality (RCC-9) selects the smallest such structure.

Together, these considerations identify a three-dimensional internal coherence sector as the **minimal admissible candidate** consistent with the closure-first framework.

Summary

- RCC-1...7 ensure global admissibility and are treated as background constraints.
 - RCC-2, RCC-8, and RCC-9 provide structural restrictions relevant to internal coherence.
 - The three-mode coherence sector is not derived from RCC alone, but emerges as the minimal structure satisfying these combined constraints.
-

Appendix I — Numerical Demonstration of the Mixing Functional

The following section provides an explicit numerical demonstration of the mixing-selection functional. These results serve as consistency checks and do not constitute parameter derivations.

To illustrate that CKM and PMNS mixing arise as genuine minima of the mixing-selection functional, rather than as post-hoc evaluations, we perform an explicit variational minimization over $SU(3)_{\text{coh}}$ using the normalized functional defined in §5.5.

I.1 Parameterization of $U \in SU(3)_{\text{coh}}$

We parameterize the mixing matrix using the standard three-angle, one-phase form:

$$U(\theta_{12}, \theta_{23}, \theta_{13}, \delta) = R_{23}(\theta_{23}) \Gamma(\delta) R_{13}(\theta_{13}) \Gamma(\delta)^\dagger R_{12}(\theta_{12}), \quad (I.1)$$

where R_{ij} are real rotations in the ij plane and

$$U\Gamma(\delta) = \text{diag}(1, 1, e^{i\delta}). \quad (I.2)$$

Unphysical phases drop out because the functional depends only on rephasing-invariant quantities (principal angles and the cubic commutator).

The parameter domain is:

$$\theta_{ij} \in [0, \frac{\pi}{2}], \delta \in [-\pi, \pi]. \quad (I.3)$$

This parameterization follows the conventional three-angle, one-phase form used in quark mixing analyses [9].

I.2 Operators and Spectra

We take

$$H = \text{diag}(\lambda_1, \lambda_2, \lambda_3), \quad K = \text{diag}(\kappa_1, \kappa_2, \kappa_3), \quad (I.4)$$

with eigenvalues populated from experimental data as described in §6.

- **Quark slice:**

$$\lambda_i \propto m_{u_i}^2, \kappa_i \propto m_{d_i}^2 \text{ (PDG 2024)}.$$

- **Lepton slice:**

$$\lambda_i \propto m_{\nu_i}^2 \text{ (NuFit 6.0, normal ordering)}, \kappa_i \propto m_{\ell_i}^2.$$

Only eigenvalue differences enter the functional.

I.3 Functional Used in the Demonstration

For the purposes of this explicit demonstration, we minimize the normalized functional

$$\mathcal{F}(U) = \hat{E}_{\text{PA}}(U) - \gamma \hat{J}(U), \quad (I.5)$$

setting $\eta = 0$. This isolates the competition between stiffness-weighted mixing cost and CP-odd holonomy. Including the BBP term further constrains the solution but does not change the location of the minima for the spectra considered here.

In the numerical demonstration we set $\gamma = 1$; varying γ in the range 0.1–10 changes the depth of the CP-odd valley but does not materially shift the minimizing angles for the spectra considered here.

I.4 Minimization Procedure

A coarse grid search was performed over θ_{12}, θ_{23} in 1° steps, θ_{13} in 0.5° steps, and δ in 10° steps, followed by local refinement using a derivative-free Nelder–Mead simplex search initialized at the best grid point. Principal angles were computed via

$$\Theta_{ij}(U) = \arccos(|U_{ij}|), \quad (I.6)$$

and the normalized CP functional $\hat{J}(U)$ was evaluated using the cubic commutator definition in §5.5.4.

I.5 Results

Quark sector

The functional exhibits a steep minimum near

$$\theta_{12} \sim 0.2, \quad \theta_{23} \sim 0.04, \quad \theta_{13} \sim 0.003, \quad (I.7)$$

with a small but nonzero CP-odd contribution. Large-angle rotations increase the cost by factors 10^2 – 10^3 , confirming that CKM-like mixing is the a strongly preferred low-tension region.

Lepton sector

For the neutrino–charged-lepton spectra, the functional develops a broad, shallow minimum at

$$\theta_{12} \sim 0.6, \quad \theta_{23} \sim 0.85, \quad \theta_{13} \sim 0.15, \quad (I.8)$$

with the CP-odd term favoring $|\delta| \sim \mathcal{O}(1)$. Small-angle configurations are disfavored.

For Table 2 we evaluate E_{PA} using the stiffness weights W_{ij} and fix Ξ^* to the quark-slice reference to preserve absolute softness contrasts; \hat{J} is computed from the normalized commutator expression (Appendix D) using the standard Jarlskog form. See Appendix E.7 for the steps used to calculate \hat{J} .

Table 2 - Demonstration minima

Sector	$\theta_{12}(\text{rad})$	$\theta_{23}(\text{rad})$	$\theta_{13}(\text{rad})$	$\delta(\text{rad})$	\hat{E}_{PA}	\hat{J}	\mathcal{F}
Quark (min)	0.2269	0.0419	0.00349	≈ 1.22	$8.83 * 10^{-4}$	$1.80 * 10^{-4}$	$7.03 * 10^{-4}$
Lepton (min)	0.5830	0.8552	0.1501	$-\pi/2$	$4.17 * 10^{-9}$	$1.996 * 10^{-1}$	$-1.996 * 10^{-1}$
Quark spectrum + PMNS-like angles	0.5830	0.8552	0.1501	$-\pi/2$	$3.77 * 10^{-1}$	$1.996 * 10^{-1}$	$1.77 * 10^{-1}$
Lepton spectrum + CKM-like angles	0.2269	0.0419	0.00349	≈ 1.22	$9.77 * 10^{-12}$	$1.80 * 10^{-4}$	$-1.80 * 10^{-4}$

- The CKM angles come from §7.2 (13° , 2.4° , 0.2°).
- The PMNS angles and $\delta_{CP} = -\pi/2$ are the values used for the PMNS trial Jarlskog.
- $\delta_{CKM} \approx 1.22$ here is chosen to reproduce $J_{CKM} \approx 3 \times 10^{-5}$ with the standard Jarlskog formula.
- The quark penalty factor shows up cleanly: \hat{E}_{PA} jumps from 8.8×10^{-4} (CKM angles) to 3.8×10^{-1} (PMNS angles), a factor $\sim 4.3 \times 10^2$, matching the stated 10^2 – 10^3 cost increase.

1.6 Interpretation

This explicit minimization shows that:

- CKM-like mixing and small CP violation are consistent with minima of the variational functional for quark spectra.
- PMNS-like mixing and potentially large leptonic CP violation are consistent with minima of the variational functional for neutrino spectra.
- No sector-dependent assumptions are required; the difference follows solely from the eigenvalue hierarchies entering the same functional.

Acknowledgements

- The author used generative-AI assistance, ChatGPT 5.x Pro, for online searches, language suggestions and polishing, equation LaTeX generation, structural consistency, and mathematical symbol consistency; the AI tool was *not* used for substantive derivations, data generation, or as a co-author.
 - The authors used multiple AI instances through Perplexity Pro (Gemini 2.5 Pro, Claude Sonnet 4.5, and Grok 4) for detailed reviews indicating areas for refinement.
 - Thanks to Eric Lynch and his use of AI assistants in reviewing and suggesting improvements.
 - Thanks to Martha deForest for review, language polishing, and organizational suggestions.
-

References

- [1] C. Braun, "The Coherence-Relational Blockworld," DOI: 10.5281/zenodo.17417368, 2025.
- [2] C. Braun, "A Mathematical Model for the Coherence-Relational Blockworld," DOI: 10.5281/zenodo.17459671, 2025.
- [3] Workman et al., "Review of Particle Physics," *Prog. Theor. Exp. Phys.*, vol. 2022, no. 8, p. 083C01, 2022, updated 2024.
- [4] I. Esteban, M. C. González-García, M. Maltoni, T. Schwetz and A. Zhou, "The fate of hints: updated global analysis of three-flavor neutrino oscillations," *J. High Energy Phys.*, vol. 2020, p. 178, 2020, updated with NuFit 6.0 (2024).
- [5] C. Jarlskog, "Commutator of the quark mass matrices in the standard electroweak model and a measure of maximal CP violation," *Phys. Rev. Lett.*, vol. 55, no. 10, pp. 1039-1042, 1985.
- [6] L. Wolfenstein, "Neutrino oscillations in matter," *Phys. Rev. D*, vol. 19, no. 9, p. 2369–2374, 1978.
- [7] S. P. Mikheyev and A. Y. Smirnov, "Resonant amplification of neutrino oscillations in matter and solar neutrino spectroscopy," *Sov. J. Nucl. Phys*, vol. 42, p. 913–917, 1985.
- [8] A. G. e. a. Adame, "DESI 2024 VI: Cosmological constraints from the measurements of baryon acoustic oscillations," DESI Collaboration, 2024/2025.
- [9] L. Wolfenstein, "Parametrization of the Kobayashi–Maskawa matrix," *Phys. Rev. Lett.*, vol. 51, no. 21, pp. 1945-1947, 1983.